2024 IEEE International Conference on Robotics and Automation (ICRA 2024)
May 13-17, 2024. Yokohama, Japan

Bio-Inspired Pupal-Mode Actuator with Ultra-Crossing Capability for Soft Robots

Zhenxing Wang, Xiao He, Yuhang Zhang, Cheng Zhang, Lei Sun, Zhidong Wang, Senior Member, IEEE, Shun Xu, and Hao Liu, Member, IEEE

***Abstract*— Robot-assisted Natural Orifice Transluminal Endoscopic Surgery (NOTES) represents a paradigm shift in surgical practice, significantly minimizing patient morbidity. However, the variability of inner diameter and the inter-luminal crossing within the luminal tracts lead to challenge for effective robotic intervention. Inspired by the motion of the chrysalis during its transformation, we designed an innovative pupal-mode actuator for NOTES robots. Through the manipulation of its internal air chambers, this actuator is capable of replicating wriggle-like movements. Through experimental analysis, we have acquired the constitutive characteristics of this actuator. Subsequently, an innovative gastric endoscopy robot is developed base the actuator and tested in a phantom. The results of the task simulations substantiate that the pupal-mode actuator has the capability to reduce resistance and enhance the safety of the endoscopic intervention.**

I. INTRODUCTION

The natural orifice transluminal endoscopic surgery (NOTES) [1] is a surgical technique that completes the surgical operation through the lumens of body (gastrointestinal tract [2], respiratory tract [3] and urological application [4]). The NOTES can minimize the trauma of surgery to patients and has broad application prospects. However, the variable inner diameter and the inter-luminal crossing lead to the difficult intervention operations and steep learning curves in NOTES.

In the past decades, various medical devices have been designed and applied in NOTES. For example, during endotracheal intubation, in order to cross the throat, a sickle shaped laryngoscope is used to achieve oropharyngeal intervention [5]; During endoscopic retrograde cholangiopancreatography (ERCP) [6], the doctors use a duodenoscopy which has a side camera and forceps lifting device, to achieve the intervention of pancreatic duct. In vascular interventional surgery, a series of guide wires, balloons, stents are used to achieve the crossing of the malformations, embolism, and valves in human blood vessels [7].

With the application of surgical robots, doctors' operational capabilities in NOTES have further improved [8]. For example, The robot-assisted bronchoscopy biopsy simplifies the physician's procedure and allows access to deeper areas of the lungs [9] [10]. DuPont et al. of Harvard Medical School designed a "wall following" algorithm [11] inspired by animals and achieved the autonomous cardiac intervention. The results of animal experiments showed that, the performance of an autonomously controlled robotic catheter rivaled that of an experienced clinician. Lucile Zorn et al. successfully performed robot-assisted ESD surgery in pigs [12]. However, the NOTES robots still need precise master-slave operation or additional assistance when facing the transition regions of the variable inner diameter and holes connecting different lumens. Especially when the lumen becomes narrow, the tip of the robot need to press the lumens to achieve the movement.

Harnessing inspiration from the natural to refine robotic design has proven to be a fruitful research method [13]–[16]. We noticed that there are many insects in nature can use simple body structure and a easy motion to drill and move in caves. For example, the chrysalis of butterflies, which have no limbs or precise perception, can complete its movement in the cave by swinging its body, as shown in Fig. 1(a, b). This pupal mode motion does not need the accurate positioning of the target hole and the accurate control of the body movement. It just needs to approach the target and wriggle the tip, keep a certain contact pressure, the body will cross various forms of holes and lumens. With the help of the soft tissue environment and the lubricating fluid in the human lumen, we believe this motion mode has great potential for the NOTES. Inspired by the chrysalis, we proposed a pupal-mode pneumatic actuator, as shown in Fig. 1. The actuator is made of silicone, and three air chambers are set inside. By controlling

*This work was supported by National Natural Science Foundationof China (Grant No.U20A20195), and the Liaoning Provincial Department of science and technology(Grant No.2021JH2/10300058), and Shenyang Bureau of Science and Technology(Grant No.21-172-9-04)

Zhenxing Wang, Xiao He, Yuhang Zhang, Cheng Zhang and Hao Liu are with the State Key Laboratory of Robotics, Shenyang Institute of Automation, Chinese Academy of Sciences, Shenyang, 110016, China; Institutes for Robotics and Intelligent Manufacturing, Chinese Academy of Sciences, Shenyang, 110016, China, and also with the Key Laboratory of Minimally Invasive Surgical Robot, Liaoning Province, Shenyang, 110016, China. Besides, Zhenxing Wang is also with University of Chinese Academy of Sciences, Beijing 100049, China. (e-mail: wangzhenxing@sia.cn, hexiao@sia.cn, zhangyuhang@sia.cn, zhangcheng@sia.cn, liuhao@sia.cn).

Lei Sun and Shun Xu are with Department of Thoracic Surgery, The First Affiliated Hospital of China Medical University, Shenyang, Liaoning, 110016 China.

Zhidong Wang is with the Department of Advanced Robotics, Chiba Institute of Technology, Narashino, Chiba, 275-0016, Japan (e-mail: zhidongwang@it-chiba.ac.jp).

*Corresponding author: Shun Xu, Hao Liu, e-mail: xushun610539@sina.com, liuhao@sia.cn

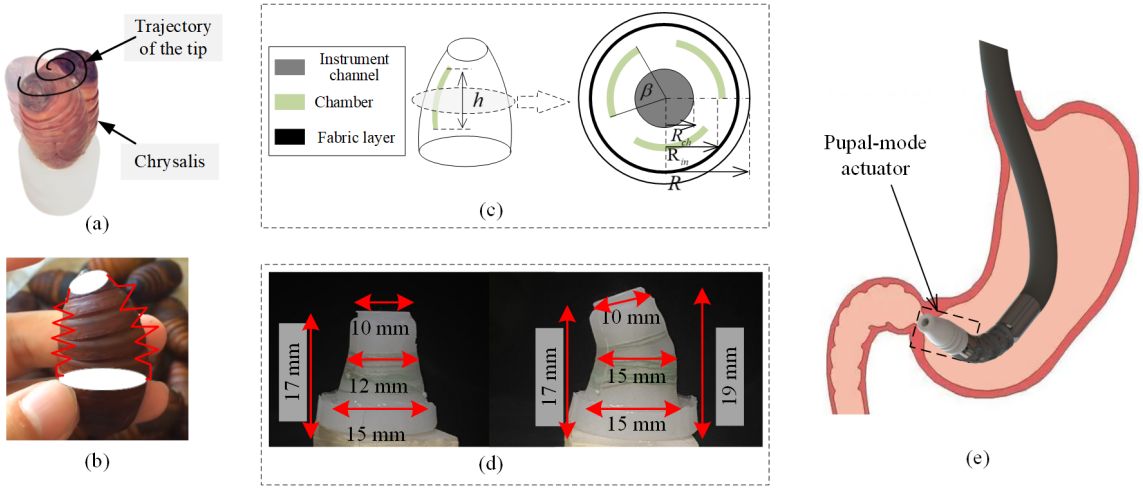

Fig. 1. The conception of the pupal-mode actuator.(a)The pupal-mode motions. (b)The mechanism of chrysalis movement. (c) Design of the pupal-mode actuator. (d)The actuator in two mode. (e)The concept for NOTEs robot.

the inflation sequence, frequency and pressure of the chambers, the actuator can reproduce the pupal motion. Further, we designed a new form of NOTES robot based on the pupal-mode actuator to verify the performance of pupal-mode actuator in NOTES, as shown in Fig. 1.e. Experiments show that the pupal motion has less interaction force and more brief control form than the traditional endoscope.

II. MATERIALS AND METHODS

A. Conception and design of the pupal-mode actuator

To begin with, we conducted an analysis of chrysalis movement and distilled the pupal-mode motion into the following design criteria:

- The base of the chrysalis should maintain stability while the head swings;
- Pupal-mode motion should incorporate two degrees of freedom (DOFs), facilitating the adjustment of frequency and amplitude in accordance with task requirements;
- The trajectories of the tip should form closed curves instead of a zigzag path for round-trip motion;

In this paper, the pupal-mode actuator is fabricated using silicone. It incorporates three internal air chambers, whose expansion induces circumferential asymmetric deformation of the actuator, resulting in lateral bending. Adhering to the first design criterion, we configured the actuator in a spindle shape with the air chamber positioned at the upper section, as shown in fig.1(c). This design provides a thicker bottom support, ensuring stability during air chamber expansion. To achieve bidirectional swinging of the actuator, the three chambers are evenly distributed circumferentially. The actuator can pivot at various angles through coordinated expansion of these chambers. The motion trajectory of the tip can be realized according to the enable sequence of these chambers, the details of the trajectory control is explained in the Section 2.C.

During chamber extension, deformation occurs in two directions, namely axial and radial. To enhance the actuator's bending efficiency, it is imperative to constrain radial deformation of the chambers. Following the approach outlined in [17], we introduced a non-elastic fabric layer into the actuator. The comprehensive design of the pupal-mode actuator is illustrated in Fig. 1(d). For the chamber design of the actuator, we drew inspiration from Wen's work [18] and described the chamber design parameters as $[K, \beta, h]$, as shown in the Fig. 1(c). The K represents the ratio of the internal thickness of the chamber $(R_{in} - R_{ch})$ to the external thickness $(R - R_{ch})$, which governs the chamber's placement in the cross-section; β signifies the central angle of the chamber cross-section; while h denotes the height from the bottom of chamber to the bottom of actuator. Based on the quantitative analysis of the chamber parameters in [18], the chamber parameters of the actuator in this paper are designed as: $K = 1.5, \beta = 90^o, h = 10mm$. The finalized actuator is shown in Fig. 1(d).

B. Fabrication

Fabricating the pupal-mode actuator posed a challenge due to the intricate internal chamber geometry, making it challenging to remove the inner mold during casting. In our study, we adopted the Lost-wax casting method, as illustrated in Fig. 2. Initially, we 3D printed the mold for the wax inner model and poured wax to create the inner wax mold, as depicted in Fig. 2(a, b, c); Subsequently, we affixed the inner model with the outer mold and poured silicone rubber (Dragon Skin 30, Smooth-On Inc.) into the model, as shown in Fig. 2(d, e); Once the silicone rubber had cured, the outer mold was removed, and a fabric layer was applied to the actuator, and a layer of silica gel was added for sealing, as shown in Fig. 2(f); Finally, the actuator was heated to melt away the

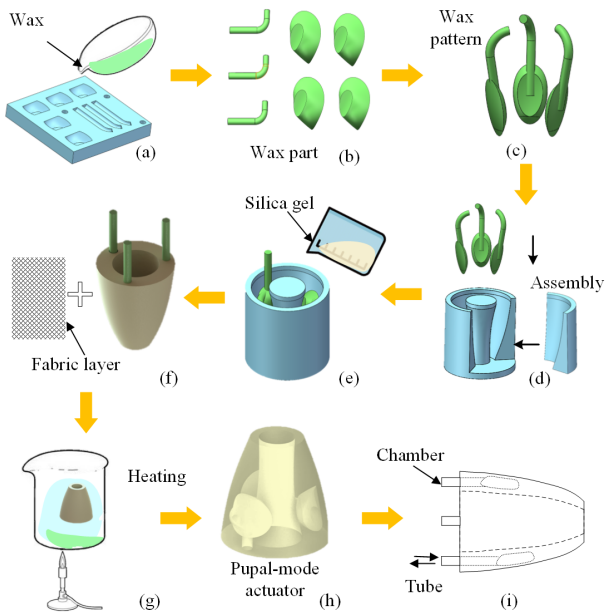

Fig. 2. The fabrication process of the pupal-mode actuator.

wax from the actuator, and gas pipes were bonded to complete the entire production process, as shown in Fig. 2(g,h,i).

C. Characterization of the pupal-mode actuator

Selection of enable sequence

The wriggle motion of the actuator is induced by the expansion of the internal chambers. Various enable sequences of the three chambers result in distinct trajectories of the actuator tip. In this study, three enable sequences were chosen, and the optimal sequence was determined by evaluating the smoothness of the trajectory. These three enable sequences are defined as follows:

$$\begin{cases} seq1, (000, 100, 110, 111, 011, 001, 000) \\ seq2, (000, 100, 000, 010, 000, 001, 000) \\ seq3, (000, 100, 110, 010, 011, 001, 101) \end{cases}$$

Where, the (XXX) represents the state of the pupal-mode actuator at a specific moment and each bit corresponds to a chamber. In this notation, 0 signifies unexpanded, while 1 indicates expansion. For example, (100) implies that the 1st chamber is expanded while the second and third chambers remain unexpanded. The Fig. 3(a) illustrates the driving process of Seq3.

We established a test platform, as depicted in Fig. 3(b). A industrial camera(H9-10, JIERUWEITONH Electronic Technology) is used to record the movement of the actuator. Three drive sequences were tested with an enabling frequency of 1 Hz and a pressure of 80 Kpa. An industrial camera was utilized to record the movement of the actuator's tip. Employing image processing techniques, we extracted the tip's contour in each frame and computed the phase angle of the current swing direction. This process is illustrated in Fig. 3(c). All image processing procedures for the experiments were conducted using MATLAB R2021a (MathWorks, Natick, MA, USA).

We employed the standard deviation of the phase velocity to assess the stability of the actuator's trajectory. First, we calculated the velocity(v_i) of the phase angle by differentiating the phase angle α with respect to time, where the i mean current frame. Subsequently, we computed the standard deviation of the velocity over a complete driving cycle as θ. The calculation process for θ is as follows:

$$\theta = \sqrt{\frac{\sum(V_i - \overline{V})^2}{N}} \tag{1}$$

Where $\overline{V}$ is the mean value of the phase velocity. The smaller the T_s value, the more stable the switching of the actuator. After calculation, the T_s of the three drive sequences are: 3.15 ± 3.34, 3.09 ± 2.74,3.11 ± 2.56. Therefore, in the subsequent experiments, we choose Seq3 as the drive order of the actuator.

Characterization of wriggle amplitude

The wriggle amplitude of the pupal-mode actuator is an important characteristic during crossing. Establishing a mapping relationship between the actuator's amplitude and the control parameters (chamber pressure and sequence frequency) serves as the foundation for actuator control. Due to the intricate shape of the gas chamber, theoretical derivation of this characterization is complex and imprecise. In this study, we conducted a series of calibration experiments to determine the relationship between the actuator's wriggle motion and the control parameters.

Utilizing the aforementioned image measurement platform, we tested the actuator at various pressure and frequency settings while recording the motion of the actuator tip. The control parameters for the actuator were selected as follows: the enable pressure ranged from 20 to 100 Kpa, and the sequence frequency ranged from 0.2 to 4 Hz.

Using the image extraction method, we extracted the area covered by the actuator tip during one cycle and calculated the minimum envelope circle of that area. The radius of this enclosing circle was chosen as the swing amplitude for that motion cycle. Due to the error of each motion cycle, we used the average of the swing amplitude in five cycles as the wriggle amplitude under this control variable, as shown in Fig. 4(a). The wriggle amplitude of the actuator's tip is positively correlated with the driving air pressure but negatively correlated with the driving frequency. The mapping of swing amplitude to pressure and frequency was experimentally determined and is depicted in Fig. 4(b). In practical applications, control parameters can be selected based on specific requirements for wriggle amplitude. We illustrate the impact of air pressure and frequency on wriggle amplitude, as shown in Fig. 4(c). with the driving air pressure

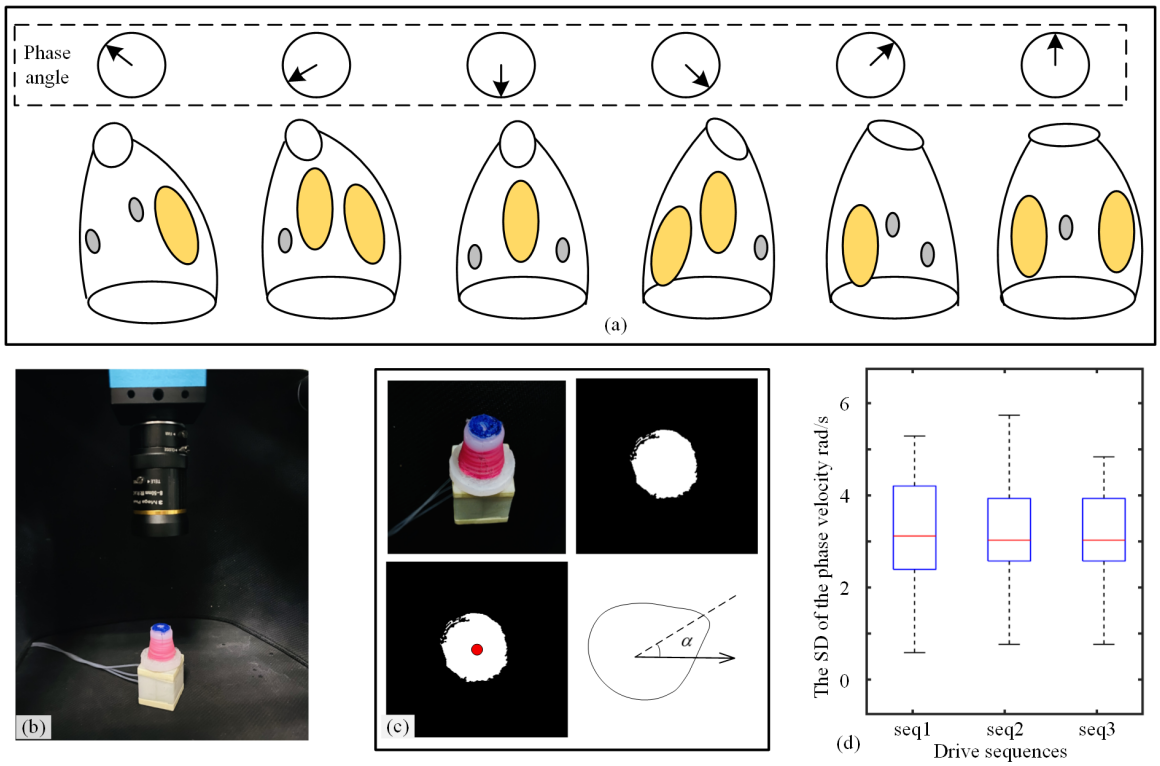

Fig. 3. The evaluation of the pupal-mode actuator drive sequences. (a) The change of the actuator in whole drive sequence (e.g. seq 3). (b)Recording the trajectory of the actuator tip; (c)The bending phase angle of the actuator. (d) The phase angular velocities of three drive sequences.

remaining constant, the wriggle amplitude gradually decreases and levels off as the driving frequency increases. At the same driving frequency, higher air pressure results in a greater swing amplitude. However. But, as the driving frequency increases, the impact of air pressure on wriggle amplitude gradually diminishes. We attribute this phenomenon primarily to the observed hysteresis in chamber expansion and contraction.

III. EXPERIMENT

In order to validate the effectiveness of the pupal-mode actuator proposed in this paper for NOTES, we designed an Duodenoscopy robot based on the proposed pupal-mode actuator. By conducting a task simulation on a phantom model of the pylorus, we recorded the intervention resistance experienced of different mode, and evaluated the effectiveness of the actuator's intervention.

A. Design of a Duodenoscopy robot

In the clinical application of digestive endoscopy [19], one of the key challenges during the operation is crossing through the pylorus, especially in cases of pyloric stenosis and pyloric tumors. In this paper, we presented a novel duodenal intervention robot which combines a pupal-mode actuator at the tip to addresses the challenges associated with pylorus intervention.

The duodenal robot comprises three components: the pupal mode actuator, the bending segment, and the endoscope-assisted segment. These components are assembled in series to form a complete robot, with a central through hole that can accommodate visual components and operating instruments. In accordance with digestive endoscopy procedures, the robot needs to possess the capability to bend and steer in two directions, which is achieved by adopted a 2-DOFs continuum structure in this paper. The endoscope-assisted segment is designed to facilitate the robot's intervention within the lengthy intestinal tract. The robot is firmly secured to a linear guide rail to enable the axial motion. The outer diameter of the robot is designed to match that of a duodenoscope at 15 mm. The length of the endoscope-assisted segment has been simplified to 200mm for the purposes of this study, focusing primarily on the evaluation of the pupal-mode actuator. An overview of the complete robot is provided in Fig. 5.

To establish the robot's kinematics, we simplified the pupal-mode actuator as follows: due to the primary function of the actuator is to enable wriggle motion rather than precise positioning, the actuator is simplified as a link in the kinematics.

The description of kinematic of the continuum segment can be found in [20]. Therefore, in this paper, we will not provide an extensive description but rather denote it as: $T_b = \begin{bmatrix} R_b & T_b \\ 0 & 1 \end{bmatrix}$. The support segment possesses only axial extension degrees of freedom, and the corre-

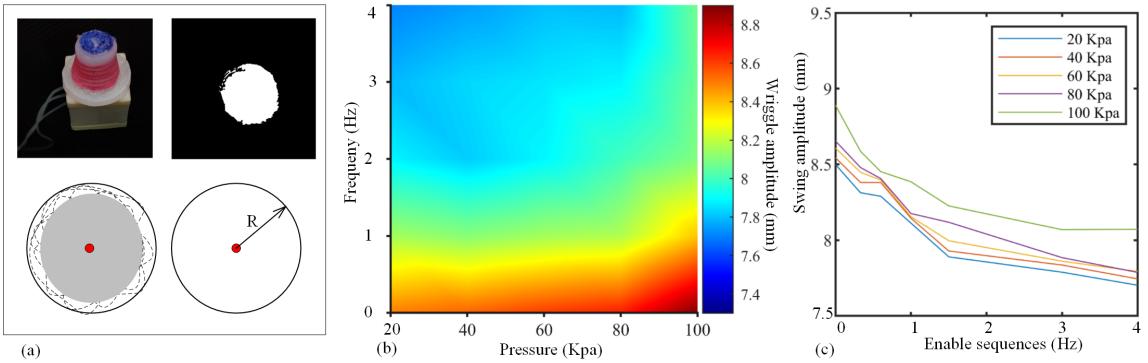

Fig. 4. The mapping of the characterization of the pupal-mode actuator. (a) The minimum envelope circle of actuator motion. (b) The mapping between swing amplitude and pressure and frequency. (c) The relationship between motion amplitude and frequency under different pressures.

sponding homogeneous transformation matrices is:$T_s = trans(z, L_s)$, the L_s segment the long of the support segment. The pose transformation matrices of the pupal-mode actuator can be expressed as: $T_t = trans(z, L_z)$. Summing up, the kinematic expression of the duodenal robot is obtained by $T = T_s T_b T_t$.

Based on the proposed duodenal robot and the kinematics model, we established a duodenal robot master-slave intervention experimental platform using a Phantom Omni device (Sensable Inc.). We also made a human digestive tract pyloric model with Dragon Skin 10, as shown in Fig. 6(a). The pyloric position of the model can be modified to simulate different pyloric conditions such as normal, stenosis and obstruction. By attaching the model to a six-dimensional force sensor(M3815B, Sunrise Instruments Inc.), we can measure the resistance encountered by the phantom during the intervention process. Based on the phantom and functional prototype, a intervention measurement platform has been established, as shown in Fig. 6(a).

B. Task simulation of the robot in gastrointestinal interventions

To assess the performance of the pupal-mode actuator of the Duodenoscopy robot during pyloric interventions, we conducted comparative evaluations of the robot and a conventional duodenoscope with the intervention measurement platform. The intervention experiments were initially conducted in a normal pyloric phantom. Both the robot and duodenoscope were operated by the same doctor. The intervention procedure involved traversing from the stomach through the pyloric segment into the duodenum, the intervention speed was controlled by the doctor mirroring clinical practices. During the experiments, the robot The robot completed intervention testing in two different modes (wriggle mode and non-wriggle mode). Each intervention mode was tested five times and the results are presented in the Fig. 6(d).

The average intervention force of the three intervention modes were as follows: 0.17 ± 0.015 N, 0.20 ± 0.025 N, and 0.21 ± 0.086 N. The intervention forces among the three modes were relatively consistent, and the variations in intervention force during a single intervention process were also quite similar, as shown in Fig. 6(d). This was primarily because the inner diameter of the pyloric region was slightly larger than the robot and duodenoscope, causing minimal obstruction during the intervention.

To further validate the intervention capabilities of the wriggle motion, we also carried out experiments in two scenarios: pyloric stenosis and pyloric tumor. The pylorus phantom is wrapped by elastic cords to simulate the pyloric stenosis cases and affixed a tumor phantom to simulate the pyloric tumor, as shown in Fig. 6(a). As the

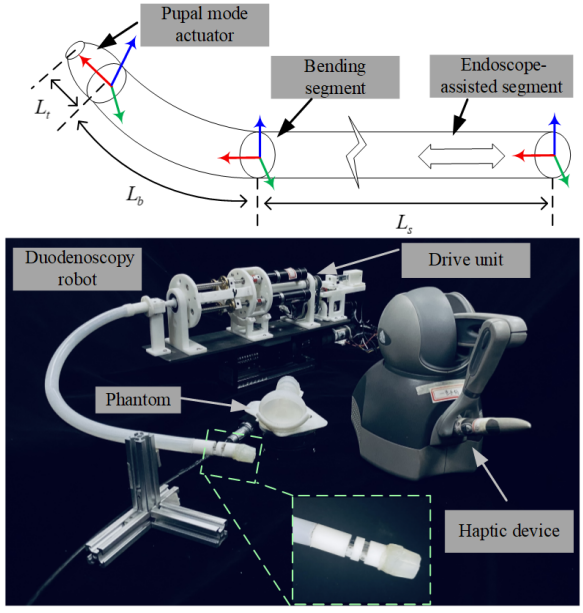

Fig. 5. The duodenoscope robot and its master-slave system.

inner diameter decreased, the intervention forces in three modes increased to 0.59 ± 0.37 N, 0.73 ± 0.44 N, 0.56 ± 0.15 N, respectively. Notably, the intervention force of the robot are consistently exceed that of duodenoscope. In a single intervention process, the force exhibited a peak before entering the pylorus in all three modes, as shown

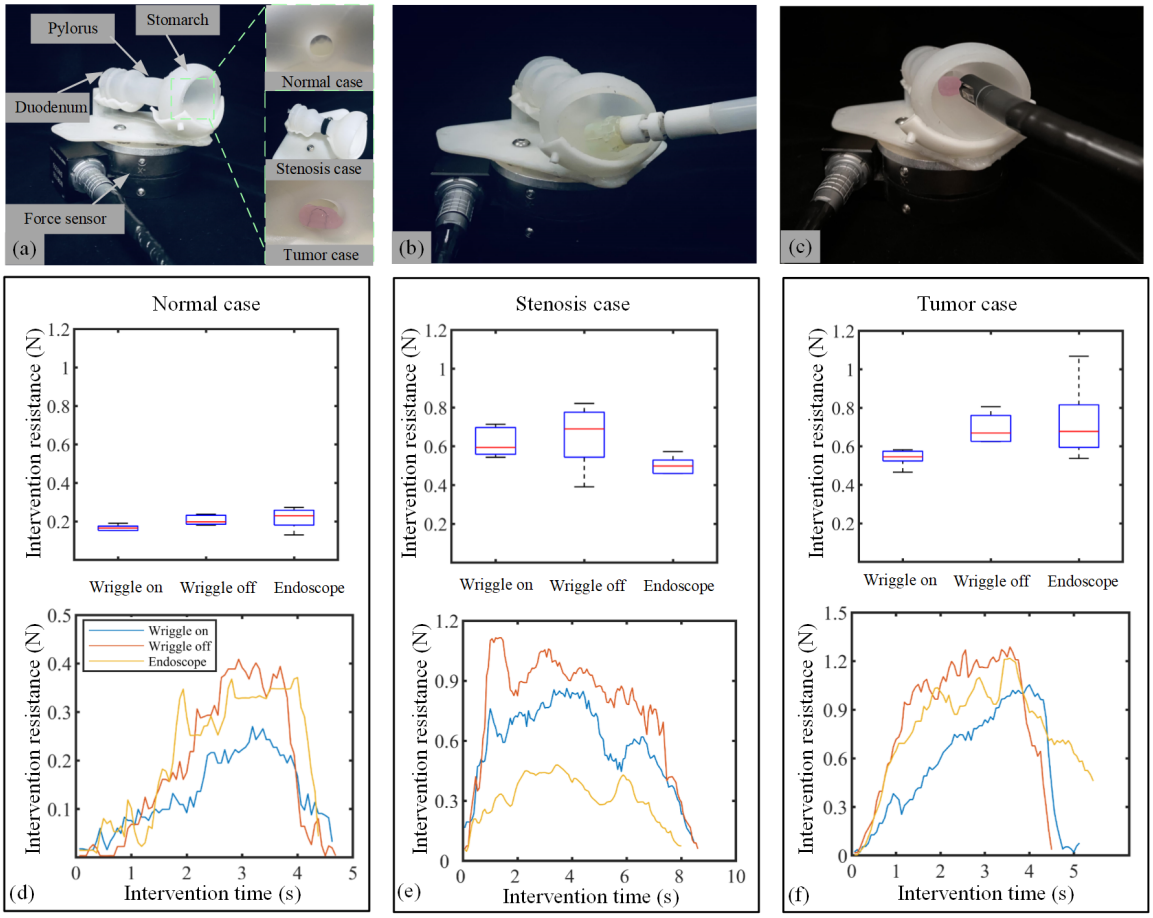

Fig. 6. Task Simulation of the Duodenoscopy Robot. (a) The Pyloric Phantom: The model is modified to simulate normal cases, stenosis cases, and tumor cases separately. (b) Robot Intervention in the Phantom. (c) Duodenoscope Intervention in the Phantom. (d) Comparison of intervention forces for the three modes in normal cases. (e) Comparison of intervention forces for the three modes in stenosis cases. (f) Comparison of intervention forces for the three modes in tumor cases.

in Fig. 6(e). Importantly, the wriggle motion significantly reduced the duration of peak resistance experienced. The reason of the increased force of the robot is the materials of actuator is soft compared to the rigid tip surface of the duodenoscope, which results the difficulty of pushing through the outer elastic cords. In the future, it will be possible to enhance the robot's intervention capability further by partially hardening the front surface of the actuator.

In the tumor cases, the average intervention forces in three modes were : 0.54±0.13 N, 0.69±0.34 N, and 0.72± 0.39 N, respectively. Notably, the robot demonstrated enhanced intervention capabilities when operating in a wriggle mode. By comparing the resistance in once operation, The wriggle motion can effectively prevents sudden spikes in intervention resistance caused by tumor obstructions. In a clinical context, this approach holds significance for preventing the rupture of tumors.

IV. CONCLUSION

Inspired by the chrysalis, this paper introduces a novel pneumatic pupal-mode actuator. The actuator incorporates three internal chambers and can replicate the wriggle motion. We established the relationships between control parameters (driving sequences, pressures, and frequencies) with the actuator's motion. Based on the pupal-mode actuator, we devised a new duodenal intervention robot and performed task simulation to analyze the robot's intervention resistance. The experiments proved the pupal-mode actuator can reduce the intervention resistance, especially when dealing with intracavity tumors.The wriggle motion proves highly effective in reducing peak contact forces, resulting in safer interventions. Overall, the pupal-mode actuator holds significant promise for applications in robot-assisted NOTES. However, there is still room for further improvement in the control model for the wriggle motion and its integration with current endoscopic technologies. Additionally, augmenting the actuator's interactive sensing to enable more autonomous intervention will be a valuable avenue for future research.

REFERENCES

[1] S. J. Bardaro and L. Swanström, "Development of advanced endoscopes for natural orifice transluminal endoscopic

surgery," *Minimally Invasive Therapy & Allied Technologies*, vol. 15, no. 6, pp. 378–383, 2006.
[2] C. G. Kim, "Natural orifice transluminal endoscopic surgery and upper gastrointestinal tract," *Journal of Gastric Cancer*, vol. 13, no. 4, pp. 199–206, 2013.
[3] C. F. Graetzel, A. Sheehy, and D. P. Noonan, "Robotic bronchoscopy drive mode of the auris monarch platform," in *2019 International Conference on Robotics and Automation (ICRA)*, pp. 3895–3901, IEEE, 2019.
[4] M. D. Tyson and M. R. Humphreys, "Urological applications of natural orifice transluminal endoscopic surgery," *Nature Reviews Urology*, vol. 11, no. 6, pp. 324–332, 2014.
[5] Y. Lim and S. Yeo, "A comparison of the glidescope® with the macintosh laryngoscope for tracheal intubation in patients with simulated difficult airway," *Anaesthesia and intensive care*, vol. 33, no. 2, pp. 243–247, 2005.
[6] V. R. Mujica and J. S. Barkin, "Occult gastrointestinal bleeding. general overview and approach.," *Gastrointestinal Endoscopy Clinics of North America*, vol. 6, no. 4, p. 833, 1996.
[7] S. Garg and P. W. Serruys, "Coronary stents, part one: Current status," *Journal of the American College of Cardiology*, vol. 56, no. 10 Suppl, 2010.
[8] C.-L. Lee, K.-Y. Wu, H. Su, S.-H. Ueng, and C.-F. Yen, "Transvaginal natural-orifice transluminal endoscopic surgery (notes) in adnexal procedures," *Journal of minimally invasive gynecology*, vol. 19, no. 4, pp. 509–513, 2012.
[9] C. F. Graetzel, A. Sheehy, and D. P. Noonan, "Robotic bronchoscopy drive mode of the auris monarch platform," in *2019 International Conference on Robotics and Automation (ICRA)*, pp. 3895–3901, IEEE, 2019.
[10] J. R. Rojas-Solano, L. Ugalde-Gamboa, and M. Machuzak, "Robotic bronchoscopy for diagnosis of suspected lung cancer: a feasibility study," *Journal of bronchology & interventional pulmonology*, vol. 25, no. 3, p. 168, 2018.
[11] G. Fagogenis, M. Mencattelli, Z. Machaidze, B. Rosa, K. Price, F. Wu, V. Weixler, M. Saeed, J. E. Mayer, and P. E. Dupont, "Autonomous robotic intracardiac catheter navigation using haptic vision," *Science robotics*, vol. 4, no. 29, p. eaaw1977, 2019.
[12] L. Zorn, F. Nageotte, P. Zanne, A. Legner, B. Dallemagne, J. Marescaux, and M. de Mathelin, "A novel telemanipulated robotic assistant for surgical endoscopy: preclinical application to esd," *IEEE Transactions on Biomedical Engineering*, vol. 65, no. 4, pp. 797–808, 2017.
[13] W. Tan, C. Zhang, R. Wang, Y. Fu, Q. Chen, Y. Yang, W. Wang, M. Zhang, N. Xi, and L. Liu, "Uncover rock-climbing fish's secret of balancing tight adhesion and fast sliding for bioinspired robots," *National Science Review*, vol. 10, no. 8, p. nwad183, 2023.
[14] C. Tang, B. Du, S. Jiang, Q. Shao, X. Dong, X.-J. Liu, and H. Zhao, "A pipeline inspection robot for navigating tubular environments in the sub-centimeter scale," *Science Robotics*, vol. 7, no. 66, p. eabm8597, 2022.
[15] Z. Gong, X. Fang, X. Chen, J. Cheng, Z. Xie, J. Liu, B. Chen, H. Yang, S. Kong, Y. Hao, *et al.*, "A soft manipulator for efficient delicate grasping in shallow water: Modeling, control, and real-world experiments," *The International Journal of Robotics Research*, vol. 40, no. 1, pp. 449–469, 2021.
[16] E. W. Hawkes, L. H. Blumenschein, J. D. Greer, and A. M. Okamura, "A soft robot that navigates its environment through growth," *Science Robotics*, vol. 2, no. 8, p. eaan3028, 2017.
[17] H. Zhao, K. O'brien, S. Li, and R. F. Shepherd, "Optoelectronically innervated soft prosthetic hand via stretchable optical waveguides," *Science robotics*, vol. 1, no. 1, p. eaai7529, 2016.
[18] Z. Xie, A. G. Domel, N. An, C. Green, Z. Gong, T. Wang, E. M. Knubben, J. C. Weaver, K. Bertoldi, and L. Wen, "Octopus arm-inspired tapered soft actuators with suckers for improved grasping," *Soft robotics*, vol. 7, no. 5, pp. 639–648, 2020.
[19] G. G. Ginsberg, M. L. Kochman, I. D. Norton, and C. J. Gostout, *Clinical Gastrointestinal Endoscopy E-Book*. Elsevier Health Sciences, 2011.
[20] R. J. Webster III and B. A. Jones, "Design and kinematic modeling of constant curvature continuum robots: A review," *The International Journal of Robotics Research*, vol. 29, no. 13, pp. 1661–1683, 2010.